Experimental investigation of bubbly flow and turbulence in hydraulic jumps

— Source link ☒

Frédéric Murzyn, Hubert Chanson

Institutions: University of Queensland

Related papers:

- Convective transport of air bubbles in strong hydraulic jumps

- Air–water interface dynamic and free surface features in hydraulic jumps

- Experimental study of the air–water shear flow in a hydraulic jump

- Le ressaut hydraulique : mesures de turbulence dans la région diphasique

- Turbulence measurements in the bubbly flow region of hydraulic jumps

ORIGINAL ARTICLE

Experimental investigation of bubbly flow and turbulence in hydraulic jumps

Frédéric Murzyn · Hubert Chanson

Abstract Many environmental problems are linked to multiphase flows encompassing ecological issues, chemical processes and mixing or diffusion, with applications in different engineering fields. The transition from a supercritical flow to a subcritical motion constitutes a hydraulic jump. This flow regime is characterised by strong interactions between turbulence, free surface and air–water mixing. Although a hydraulic jump contributes to some dissipation of the flow kinetic energy, it is also associated with increases of turbulent shear stresses and the development of turbulent eddies with implications in terms of scour, erosion and sediment transport. Despite a number of experimental, theoretical and numerical studies, there is a lack of knowledge concerning the physical mechanisms involved in the diffusion and air–water mixing processes within hydraulic jumps, as well as on the interaction between the free-surface and turbulence. New experimental investigations were undertaken in hydraulic jumps with Froude numbers up to Fr = 8.3. Two-phase flow measurements were performed with phase-detection conductivity probes. Basic results related to the distributions of void fraction, bubble frequency and mean bubble chord length are presented. New developments are discussed for the interfacial bubble velocities and their fluctuations, characterizing the turbulence level and integral time scales of turbulence representing a "lifetime" of the longitudinal bubbly flow structures. The analyses show good agreement with previous studies in terms of the vertical profiles of void fraction, bubble frequency and mean bubble chord length. The dimensionless distributions of interfacial velocities compared favourably with wall-jet equations. Measurements showed high turbulence levels. Turbulence time scales were found to be dependent on the distance downstream of the toe as well as on the distance

F. Murzyn (✉)
ESTACA Campus Ouest, Parc Universitaire de Laval – Changé, RueGeorges Charpak,
BP 53061 Laval Cedex 9, France
e-mail: fmurzyn@estaca.fr

H. Chanson
Division of Civil Engineering, School of Engineering, The University of Queensland, Brisbane,
QLD 4072, Australia
e-mail: h.chanson@uq.edu.au

to the bottom showing the importance of the lower (channel bed) and upper (free surface) boundary conditions on the turbulence structure.

Notations

C	Void fraction defined as the volume of air per unit volume of mixture
C_{max}	Maximum void fraction in the air bubble diffusion layer
D_t	Turbulent diffusivity (m^2/s) of air bubbles in air–water flow
D^*	Dimensionless turbulent diffusivity: $D^* = D_t/(U_1 d_1)$
d_{mbcl}	Mean bubble chord size (m)
d_1	Upstream flow depth (m)
F	Bubble count rate (Hz) or bubble frequency
F_{max}	Maximum bubble count rate (Hz) at a given cross-section
Fr	Upstream Froude number
g	Acceleration of gravity: $g = 9.80\,m/s^2$ in Brisbane (Australia)
h_c	Channel height (m)
L_c	Channel length (m)
l_c	Channel width (m)
N_{ab}	Number of air bubbles per record
Q	Water discharge (m^3/s)
Re	Reynolds number ($Re = \rho U_1 d_1/\mu$)
R_{xx}	Normalised auto-correlation function (reference probe)
R_{xz}	Normalised cross-correlation function between two probes output signals
$(R_{xz})_{max}$	Maximum cross-correlation coefficient between two probes output signals
Tu	Measure of the turbulence level in the air–water flow
T_{xx}	Auto-correlation integral time scale (s)
$T_{0.5}$	Characteristic time lag for which $R_{xx} = 0.5$ (s)
U_1	Depth-averaged flow velocity upstream of the hydraulic jump
V	Interfacial velocity (m/s)
V_{max}	Maximum velocity measured in a cross-section (m/s)
x	Longitudinal distance from the upstream gate (m)
x_1	Longitudinal distance from the gate to the jump toe (m)
y	Distance measured normal to the bed channel (m)
y^*	Distance measured normal to the channel bed corresponding to the boundary between the turbulent shear layer and the mixing layer
y_{Cmax}	Distance normal to the jet support where $C = C_{max}$
y_{Fmax}	Distance normal to the jet support where $F = F_{max}$
z	Transverse distance from the channel centreline

Greek symbols

δ	Boundary layer thickness (m)
μ	Dynamic viscosity of water (Pa s)
ρ	Density of water (kg/m^3)
Δx	Longitudinal distance between probe sensors (m)
$\tau_{0.5}$	Characteristic time lag for which $R_{xz} = 0.5(R_{xz})_{max}$

Subscript

1   Upstream flow conditions

1 Introduction

A hydraulic jump is the sudden transition from a supercritical open-channel flow regime to a subcritical regime. It is characterised by a highly turbulent flow with an air–water shear layer and a recirculating area. Macro-scale vortices develop in the roller region and interact with the free surface. Beyond the region of turbulence production next to the impingement point, significant kinetic energy dissipation takes place. In terms of environmental aspects, this property is used, for instance, with low impact structures for river restoration. Hydraulic jumps are aimed to maximise energy dissipation and to minimize flood damages. In the two-phase flow region, the strong interactions between turbulence and the free surface lead to splashes and droplet ejections. Figure 1 shows a sketch of a hydraulic jump with the relevant notations. Figure 2 presents typical vertical void fraction and bubble frequency profiles in the jump roller.

   The main parameter which characterises a hydraulic jump is its Froude number (Fr) defined as:

$$\mathrm{Fr} = \frac{U_1}{\sqrt{gd_1}} \tag{1}$$

where U_1 is the inflow velocity (m/s), d_1 is the inflow water depth (m) and g is the gravity acceleration (m/s^2). For a hydraulic jump, the Froude number is always greater than unity. Previous studies showed that air entrainment starts for $1 < \mathrm{Fr} < 1.3$ [3,20,24]. The mixing of air and water is caused by the strong interactions between turbulence and the free surface which generates disturbances of the air–water interface and vortex formation. An understanding of the basic physical mechanisms is critical because they govern the mixing, diffusion and transfer processes with applications in river restoration design tools, oxygen transfer and air/sea exchanges (hydraulic jumps may be considered as a steady spilling breaker). They
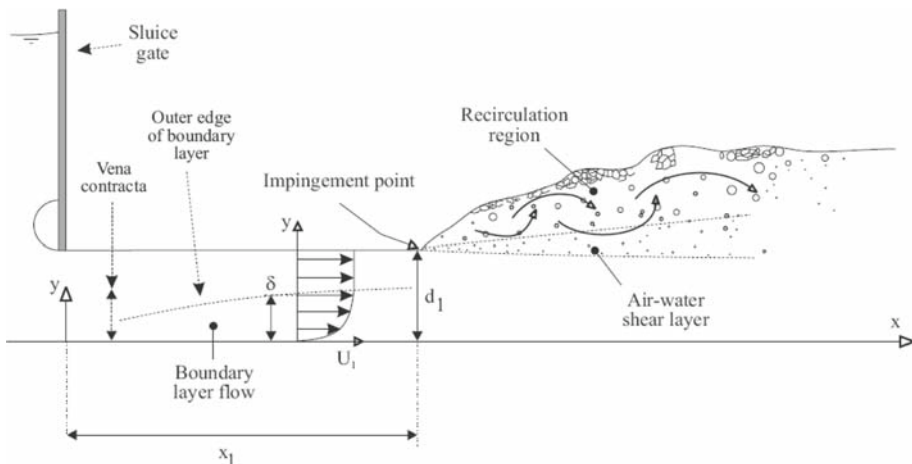

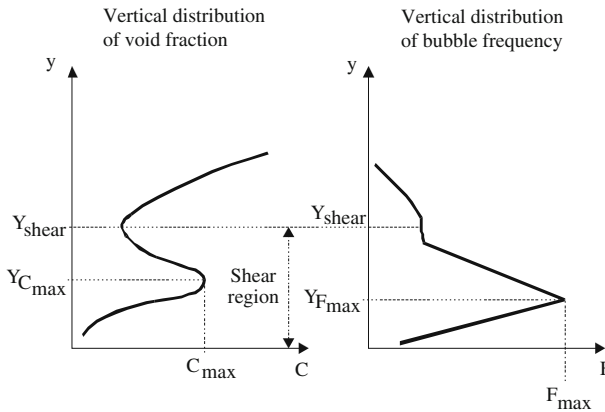**Fig. 1** Definition sketch of a hydraulic jump

Fig. 2 Vertical distributions of void fraction (C) and bubble count rate (F) in a hydraulic jump

also influence the rate of energy dissipation [5]. Studies of hydraulic jumps have a broad range of applications and results may be helpful for studies on wall-jet flows (similitude of velocity profiles), and self-aerating flows (in terms of experimental technique improvements for instance) with direct applications for coastal, river and chemical engineering purposes.

Void fraction measurements in hydraulic jumps were first conducted by Rajaratnam [26]. Ten years later, Resch and Leutheusser [28] performed hot-film probe measurements in the bubbly flow region showing the effects of the upstream flow conditions. In the last decade, a number of researchers studied the air/water properties (void fraction, bubble frequency, bubble size etc) and the free surface behaviour (length and time scales, frequency range). Recently, turbulence properties inside the water column were also studied. The most significant contributions included [2,19,10], and [24,25]. These studies highlighted important features:

A. The importance of the maximum void fraction (C_{max}) in the turbulent shear layer in hydraulic jumps with partially developed inflow conditions [2];

B. The decay of this maximum of void fraction (C_{max}) with increasing downstream distance from the jump toe [10];

C. The distinction in two regions of the vertical void fraction profiles measured in the roller (Fig. 3). The first one extends from the bottom of the channel to a well-defined position $y = y^*$. On this region, the void fraction profile satisfies a diffusion equation [3]. This was experimentally verified by Chanson and Brattberg [10] and Murzyn et al. [24]. This region is called the turbulent shear layer. The second region extends from y^* up to the free surface. In this part, the air content is strongly dominated by interfacial aeration and large amplitude of the free surface motion. [24] suggested that, in this upper part, void fraction profiles are best fitted by a Gaussian error function;

D. The strong turbulence levels in the turbulent shear flow. Rouse et al. [30], Resch and Leutheusser [28,29], Chanson and Brattberg [9,10], Liu et al. [18], Mouazé et al. [20, 21], Chanson [6,7], Kucukali and Chanson [17], Murzyn and Chanson [23] gave important contributions on turbulence levels, air–water turbulence length and time scales developing at the free surface. [21] identified some turbulent length scales associated with the free surface fluctuations along the hydraulic jumps using wire gages and video analysis for low Froude numbers (2 < Fr < 4.8) while the study of Chanson and Brattber [10] covered larger Froude numbers (Fr = 6.3 and Fr = 8.5);
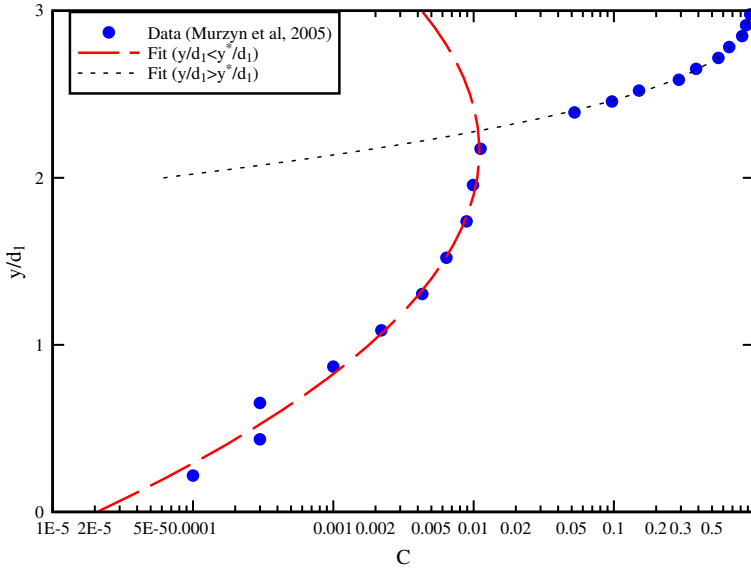
Fig. 3 Typical vertical void fraction profile in hydraulic jump (from [24])

   E. The importance of dynamic similarity (Froude) and scale effects between models and prototypes that must be taken into account for an accurate description of two-phase flow properties in hydraulic jumps [6,8].

This paper aims to present new developments on turbulence characterisation in hydraulic jumps with relatively large inflow Froude numbers ($5.1 \leq \text{Fr} \leq 8.3$), with a special interest on air–water flow properties, interfacial velocities and turbulence properties. Table 1 summarises the flow conditions of some relevant earlier studies and the present one. The experimental facility is presented in part 2 with the instrumentation, data analysis techniques and flow conditions. Part 3 describes the results. The last part of the present paper discusses some conclusions in the context of "multiphase flows in environmental problems". A brief description of future works is also proposed.

2 Experimental set-up and flow conditions

2.1 Experimental set-up

The present experiments were undertaken in a horizontal rectangular flume at the Gordon McKAY Hydraulics Laboratory of the University of Queensland (UQ). The channel width was $l_c = 0.50$ m, its length was $L_c = 3.20$ m and its height is $h_c = 0.45$ m. The sidewalls were made of glass and the bed was made of PVC. The water discharge was measured with a Venturi meter located in the supply line which was calibrated on-site with a large V-notch weir (accuracy: $\pm 2\%$). A vertical gate with a rounded shape allowed the formation of the hydraulic jump (Figs. 1 and 4). Further details on the experimental facility were reported in Murzyn and Chanson [23].

   A dual-tip conductivity probe manufactured at the University of Queensland was used to record the air–water flow properties (Fig. 5a). It was a phase detection intrusive probe designed

Table 1 Experimental conditions of previous and present investigations in hydraulic jumps with partially developed inflow conditions

References (1)	Fr (2)	Re (3)	d_1 (m) (4)	x_1 (m) (5)	Measurement technique (s) (6)
[9,10]	6.33–8.48	33,000–44,000	0.014	0.50	Double-tip conductivity probe 0.025 mm inner electrode 8 mm tip spacing
[24]	2.0–4.8	46,000–88,000	0.021–0.05		Double-tip optical fiber probe 0.010 mm diameter 1 mm tip spacing
[6]	5–8.6	25,000–98,000	0.013–0.029	0.5–1.0	Two single-tip conductivity probes 0.35 mm inner electrode
[17]	4.7–8.5	50,000–100,000	0.024	1.0	Conductivity probes + single tip probe, 0.35 mm inner electrode + double-tip probe, 0.25 mm inner electrode, 7.0 mm tip spacing Ultrasonic displacement meters
Present study	5.1–8.3	38,550–64,100	0.018	0.75	Double-tip conductivity probe 0.25 mm inner electrode 7.0 mm tip spacing

Fig. 4 Hydraulic jump in the experimental facility at the University of Queensland (flow from right to left, Fr = 5.1)

to pierce the bubbles and its principle was based on the difference between electrical resistance of air and water [4,12]. The streamwise distance between probe sensors was $\Delta x = 7$ mm (Fig. 5b). The response time of this sensor was $<10\mu$s. The signal output was scanned for 45 s at 20,000 Hz per sensor. The sampling rate and sampling duration were chosen according to the quality control procedure developed by [31] and [6,8] The data accuracy was on the void fraction $\Delta C = 2\%$, on the bubble frequency $\Delta F/F = 0.5\%$, on the mean bubble chord
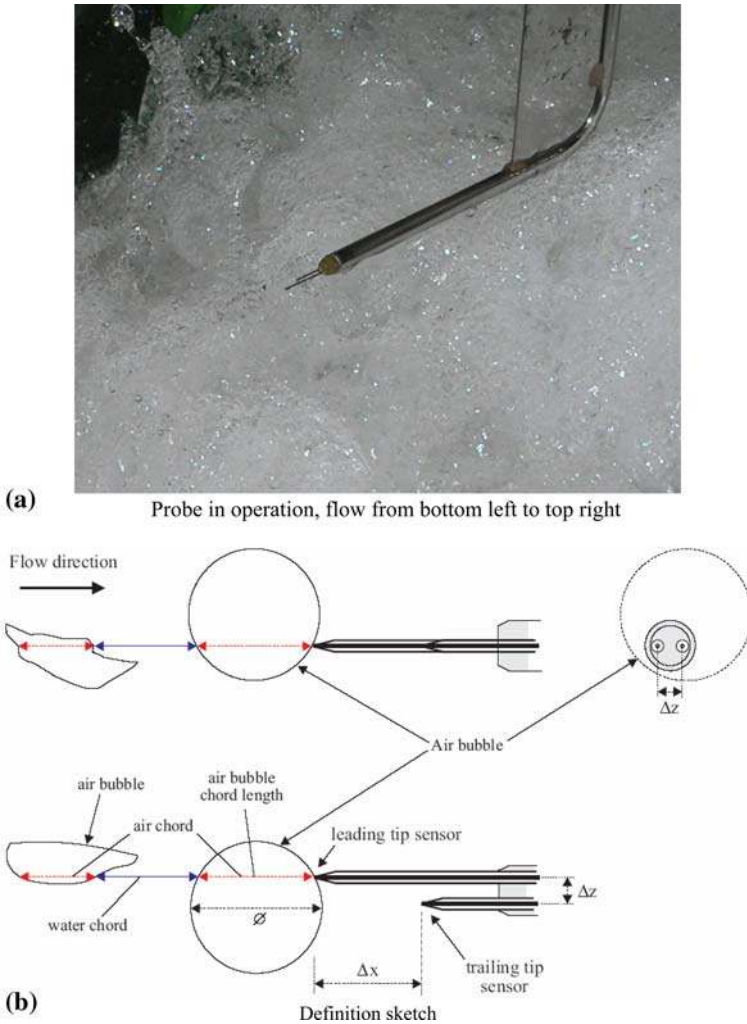
Fig. 5 Dual-tip conductivity probe (**a**) Probe in operation, flow from bottom left to top right (**b**) Definition sketch

length $\Delta d_{mbcl} = 0.2$ mm and on the interfacial velocity $\Delta V/V = 5\%$ (if $0.05 < C < 0.95$) or 10% (if $C < 0.05$ or $C > 0.95$). Depending on the upstream Froude number, three to four vertical profiles were recorded at different cross-sections downstream of the jump toe. Each profile contained at least 30 points. The step between 2 points ranges from 3 mm (closed to the bottom) to 10 mm in the upper part of the flow. Figure 6 presents a typical voltage output of the conductivity probe leading sensor. The high voltage level corresponds to water whereas the lower level is relative to air. The distinction between both phases was performed using a single threshold technique [31].

The main properties of the air–water flow were calculated. These included the void fraction (C), bubble count rate (F), mean bubble chord length (d_{mbcl}), interfacial velocity (V), turbulence levels (Tu) and turbulence time scales (T_{xx}), defined as:
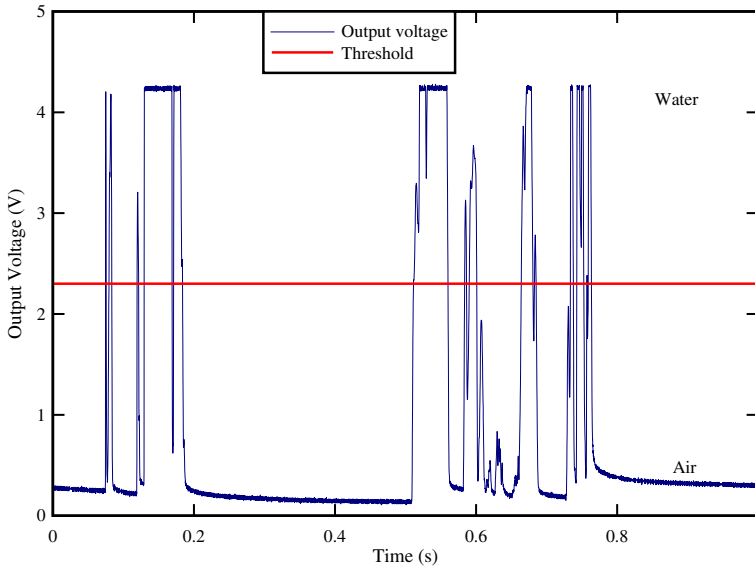
Fig. 6 Voltage output from conductivity probe

$$V = \frac{\Delta x}{T} \tag{2}$$

$$Tu = 0.851 \frac{\sqrt{\tau_{0.5}^2 - T_{0.5}^2}}{T} \tag{3}$$

$$T_{xx} = \int_{\tau=0}^{\tau=\tau(R_{xx}=0)} R_{xx}d\tau \tag{4}$$

where Δx is the longitudinal distance between probe sensors, T is the average air–water interfacial travel time between the two sensors, $\tau_{0.5}$ is the time scale (s) for which the nor-malised cross-correlation function is half of its maximum value such as $R_{xz}(T + \tau_{0.5}) = (R_{xz})_{max}/2$, $(R_{xz})_{max}$ is the maximum cross-correlation coefficient for $\tau = T$, $T_{0.5}$ is the time (s) for which the normalised auto-correlation function equals 0.5, R_{xx} is the normalised auto-correlation function of the probe signal.

The turbulence level Tu corresponds to the fluctuations of the air–water interfacial velocity and T_{xx} is an integral time scale representing the longitudinal bubbly flow structures [7,11].

2.2 Flow conditions

The experimental conditions are summarised in Table 2 where Q is the discharge (m^3/s) and Re is Reynolds number defined as $Re = \rho U_1 d_1 / \mu$, ρ and μ being respectively the density (kg/m^3) and the dynamic viscosity of water (Pas). For all conditions, the toe of the jump was stable fixed at $x_1 = 0.75$ m. The flume was relatively short and the flow was bounded by the upstream vertical sluice gate and a downstream adjustable overflow sharp-crested gate. This yielded small oscillations of the toe (± 5 cm in amplitude) with fluctuation frequencies from 1 to 3 Hz. The measured inflow depth was $d_1 = 0.018$ m. The corresponding inflow conditions were partially developed ($\delta/d_1 < 1$).

Table 2 Experimental conditions for air–water flow measurements

Test	Q (m^3/s)	U$_1$ (m/s)	Fr	Re	x − x$_1$ (m)	x − x$_1$ (m)	x − x$_1$ (m)	x − x$_1$ (m)
1	0.019	2.12	5.1	38150	0.075	0.150	0.225	–
2	0.029	3.18	7.6	57250	0.225	0.300	0.450	–
3	0.031	3.47	8.3	62250	0.225	0.300	0.450	0.600

3 Results

3.1 Bubbly flow

The basic air/water flow properties are described herein. Figures 7–9 illustrate typical vertical distributions of void fraction (C), bubble frequency (F) and mean bubble chord length d$_{mbcl}$, respectively.

Figure 7 shows some vertical profiles of void fraction at different longitudinal positions $(12.5 < (x − x_1)/d_1 < 33.3)$ downstream of the toe for one inflow Froude number (Fr = 8.3). In this figure, the dashed lines ("theory") refer to the solution of the diffusion equation presented by [3]:

$$C = C_{max} \exp \left(- \frac{\left(\frac{y - y_{C_{max}}}{d_1} \right)^2}{4D^* \left(\frac{x - x_1}{d_1} \right)} \right) \tag{5}$$

where D* is the dimensionless turbulent diffusivity, C$_{max}$ is the maximum void fraction in the shear layer measured at a distance y$_{C_{max}}$ above the bottom. The results (Fig. 7) highlighted some similar shape for all positions as illustrated in Fig. 2 (left part). All profiles clearly exhibited a marked peak in void fraction (C$_{max}$) in the turbulent shear layer. The vertical
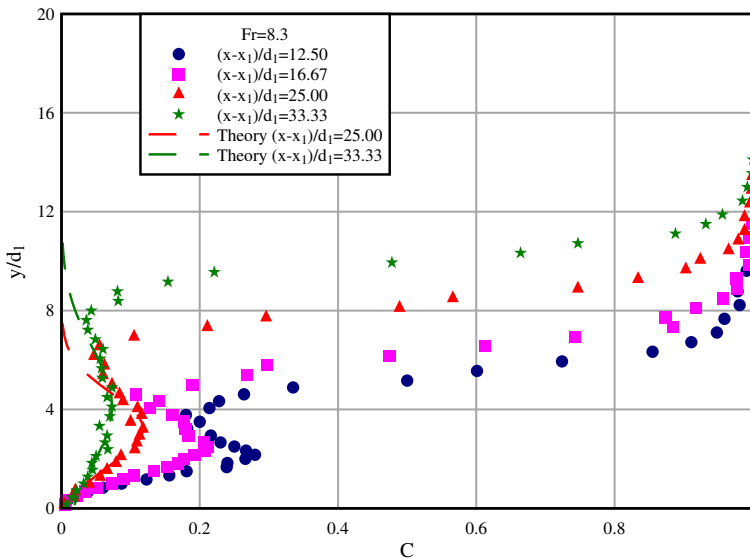

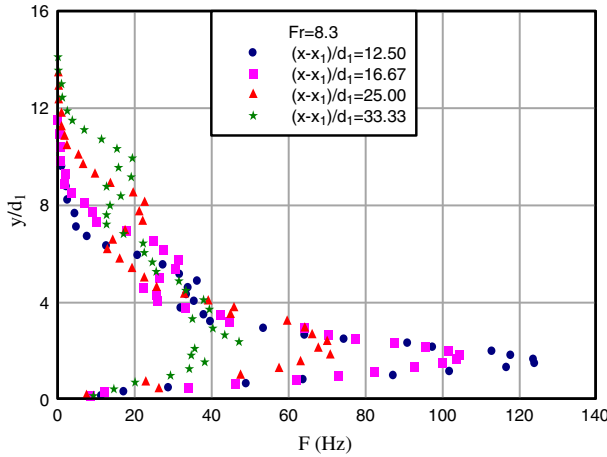**Fig. 7** Vertical profile of air concentration for Fr = 8.3

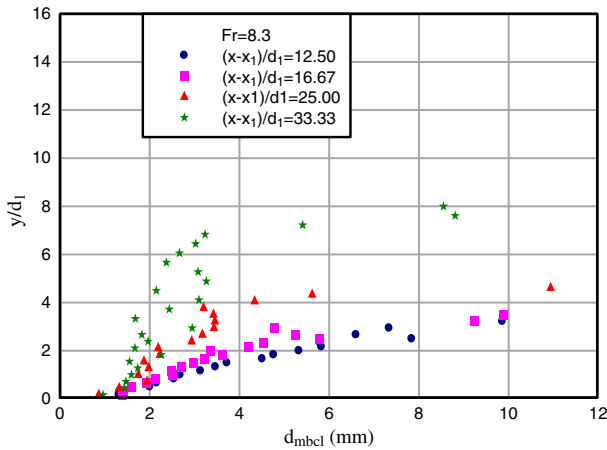**Fig. 8** Vertical profile of bubble frequency for Fr = 8.3

Fig. 9 Vertical profile of mean bubble chord length for Fr = 8.3

position of this maximum of void fraction $(y_{C_{max}}/d_1)$ increased with increasing distance to the jump toe. The present data compared favourably with the data of [9,10] and [17]. The best data fit was given by:

$$\frac{y_{C_{max}}}{d_1} = 1 + 0.11 \frac{x - x_1}{d_1} \tag{6}$$

This result is related to buoyancy effects which became predominant when the distance from the toe increased. Further, the maximum void fraction (C_{max}) decreased with increasing distance from the toe and the data were best correlated by:

$$C_{max} = 0.07 \text{ Fr } \exp\left(-0.064 \frac{x - x_1}{d_1}\right) \tag{7}$$

Far from the toe, very small values of C_{max} were observed and the vertical profile became nearly flat. The same pattern was observed for all Froude numbers (Fr = 5.1, 7.6 and 8.3).

Figure 8 presents four vertical profiles of bubble frequency (F) corresponding to four longitudinal positions downstream of the toe ($12.5 < (x - x_1)/d_1 < 33.3$). The data denoted a trend which was in good agreement with earlier investigations [7,9,10,17] and sketched in Fig. 2 (right). At each cross section, the bubble frequency profiles showed two distinctive maxima of bubble frequency. A major peak (F_{max}) was located in the developing turbulent shear layer while the second (minor peak) was found next to the upper free-surface. The results showed that the largest bubble count rate data were found close to the jump toe. The maximum bubble frequency decreases with increasing the distance to the toe. The result is in agreement with the findings of Chanson and Brattberg [10]. All the data relative to the dimensionless maximum bubble count rate data were accurately defined by the empirical correlation:

$$\frac{F_{max} d_1}{U_1} = 0.117 \ \text{Fr} \ \exp\left(-0.0415\frac{x - x_1}{d_1}\right) \tag{8}$$

The vertical position of the maximum of bubble frequency (y_{Fmax}/d_1) increased with increasing the distance from the toe. A close comparison between Figs. 7 and 8 shows that the position of the maximum of void fraction (y_{Cmax}/d_1) was always above the position of maximum bubble frequency (y_{Fmax}/d_1). That is: $y_{Fmax}/d_1 < y_{Cmax}/d_1$. This trend was observed for all inflow Froude numbers and previously highlighted by Chanson and Brattberg [10]. The difference between the positions of the maxima in void fraction and bubble frequency (y_{Cmax}/d_1, y_{Fmax}/d_1) characterised some double diffusion process. Based on previous works [6,10], it is suggested that vorticity and air bubbles diffuse at a different rate and in a different manner downstream of the impingement point. The asymmetry in the turbulent shear stress across the bubbly flow region would influence the mean bubble chord length and hence the number of bubbles for a given void fraction in the advective diffusion region.

Figure 9 shows some vertical profiles of mean bubble chord length (d_{mbcl}) for Fr = 8.3 at several distances from the toe ($12.5 < (x - x_1)/d_1 < 33.3$). The mean bubble chord length was typically between 1 and 8 mm. The results implied that the smallest bubbles were found in the lower part of the flow ($y < y_{Cmax}$). At a given position ($x - x_1)/d_1$ in the roller, the trend was nearly linear for all Froude numbers. The range of mean bubble chord length was also in good agreements with previous studies [7,24] for similar Froude numbers. The largest bubbles are found close to the free surface where the shear is smaller. Flow visualizations also confirm these results.

3.2 Interfacial velocities, turbulence levels and time scales

The distributions of dimensionless interfacial velocity, turbulence level and integral turbulent time scale in the hydraulic jump are presented in Figs. 10–12. The data analysis was based upon a cross-correlation technique between the two conductivity probes according to Eqs. 2–4. The turbulence level corresponded to the fluctuations of the interfacial velocity [1,4,11].

Figure 10 presents the dimensionless distributions of the interfacial velocity V/V_{max} for Fr = 8.3 and $12.5 < (x - x_1)/d_1 < 25$. These results are restricted to the region where the velocity was positive and the probe sensors were aligned with the flow streamlines. In the upper part of the flow, data were meaningless because of the reverse flow associated with negative velocities. It must be mentioned that our technique is intrusive and thus disturbs the flow (weak effects). Nevertheless, in the lower part of the flow, velocities were large enough ($V > 1$ m/s) and the dimensions of the sensors were small enough compared to the scales of the flow (Table 1) to ensure the accuracy and the quality of the results. All vertical profiles
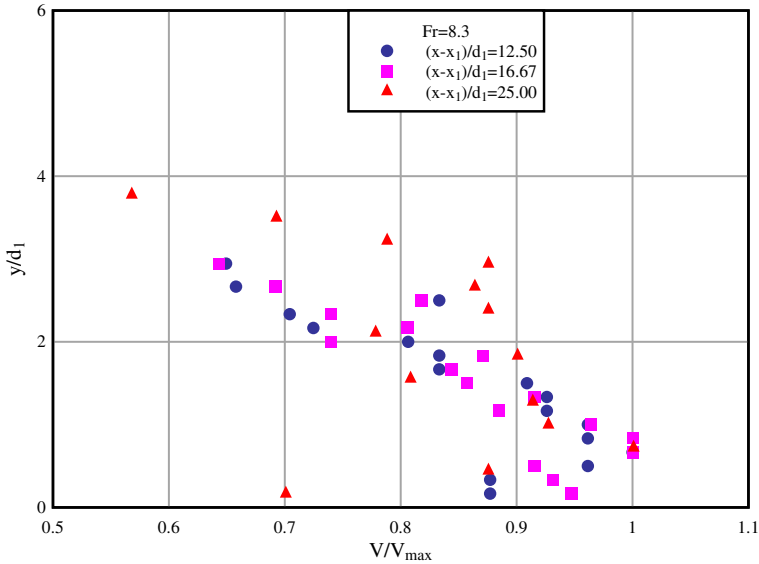
Fig. 10 Dimensionless distributions of interfacial velocity V/V_{max} in hydraulic jump for $Fr = 8.3$

indicated the presence of a boundary layer close to the bottom characterized by a rapid increase in the dimensionless interfacial velocity until a maximum velocity at $y = y_{V_{max}}$. Above this position, a gradual decrease in velocity was observed with increasing distance from the bed. Similar shapes were found regardless of the position $(x - x_1)/d_1$. These results tended to confirm that the velocity profiles were close to those observed in wall-jet flows [10,27]:

$$\frac{V}{V_{max}} = \left(\frac{y}{y_{V_{max}}}\right)^{1/N}, \quad \text{for } y < y_{V_{max}} \tag{9a}$$

$$\frac{V}{V_{max}} = \exp\left(-\frac{1}{2}\left[1.765\left(\frac{y - y_{V_{max}}}{y_{0.5}}\right)\right]^2\right), \quad \text{for } y_{V_{max}} < y < 4y_{V_{max}} \tag{9b}$$

where V_{max} is the maximum velocity measured at $y = y_{V_{max}}$, $y_{0.5}$ is the vertical elevation where $V = 0.5\,V_{max}$ and N is nearly constant ($N \sim 6$). The trends given by Eq. 9 were clearly identified despite some data scatter caused by the unsteady and fluctuating nature of the flow. Far downstream (of the roller), vertical velocity profiles recovered typical shapes corresponding to free surface open channel flows.

Figure 11a–c show large turbulence levels in the hydraulic jumps up to 400% which increased with increasing distance from the bed. Tu increased also with increasing Froude number at a given position downstream of the toe. In the roller, at a given position $(x - x_1)/d_1$, the maximum turbulence level was found to be close to the free surface showing that the dynamics of the free surface strongly affected the fluctuations of the interfacial velocity and thus the dynamics of the flow. This point is particularly known in wavy free surface flows [22]. In hydraulic jumps, the same pattern was found. The free surface interacted with the flow as large air packets were entrapped from above, leading to higher levels of turbulence below the free surface. For all experiments, the turbulence level profile became nearly uniform at the largest distance to the toe. This was expected as the flow recovered lower fluctuating levels.
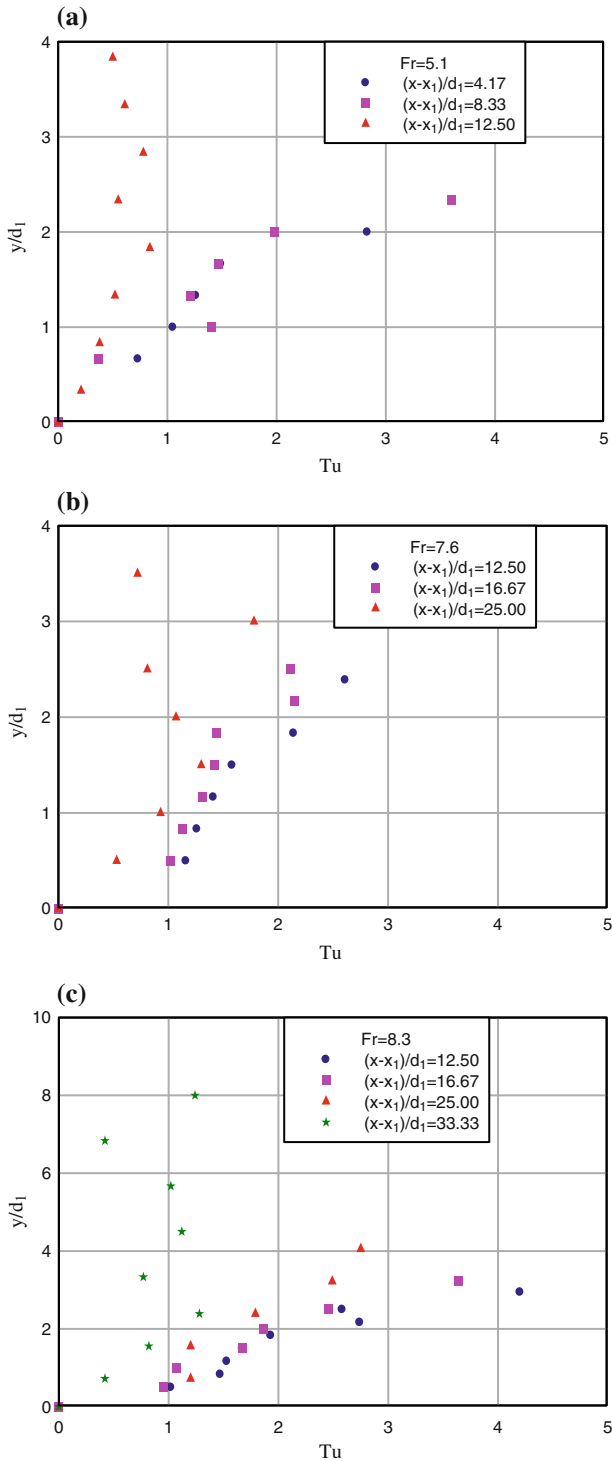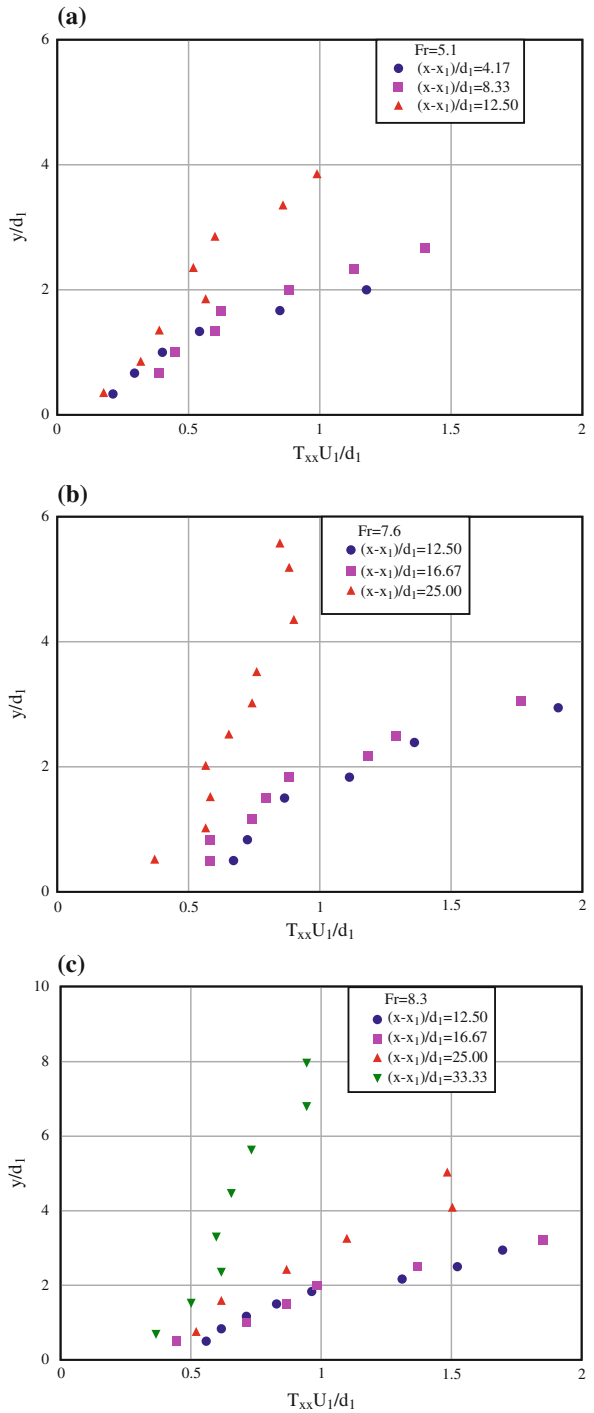
(a)

(b)

(c)

Fig. 11 Vertical profiles of turbulence intensity in hydraulic jumps (**a**) Fr = 5.1 (**b**) Fr = 7.6 (**c**) Fr = 8.3

Fig. 12 Vertical profiles of integral time scale of turbulence in hydraulic jumps (**a**) Fr = 5.1 (**b**) Fr = 7.6 (**c**) Fr = 8.3

Another relevant property was the integral time scale of turbulence which characterised some "lifetime" of the longitudinal bubbly flow structures. Figures 12a–c present some vertical profiles of dimensionless time scale $T_{xx}U_1/d_1$. The vertical profiles became nearly uniform at the largest distances to the jump toe. The smallest time scales were found close to the channel bed suggesting that the bottom imposed some boundary condition which blocked the vortex development and stretching. Previous results showed that the free surface could play a similar role, although with a lesser influence [22]. Hence at a given position $(x-x_1)/d_1$, the longest "lifetimes" were found close to the free surface. This indicated that the largest structures developed in the turbulent shear layer and above.

4 Summary and conclusions

The present study investigated the air/water flow and turbulence properties in hydraulic jumps. The measurements were performed in the experimental facility of the University of Queensland. The Froude number ranged from 5.1 to 8.3. The present study brings new important information for hydraulic researchers and highlights the complex nature of the flow. The main outcomes can be summarised as:

– The vertical void fraction profiles may be separated in two regions: the turbulent shear layer and an upper part strongly influenced by the free surface. The finding was in good agreement with previous studies;
– The maxima of void fraction (C_{max}) and bubble frequency (F_{max}) were found in the developing shear region at two different vertical distances above the bed ($y_{Fmax}/d_1 < y_{Cmax}/d_1$) indicating two competitive turbulent processes. This was also in good agreement with previous studies;
– New interesting developments were related to the distributions of interfacial velocity and turbulence levels (fluctuation of the interfacial velocity). Vertical interfacial velocity profiles were found to be similar to those obtained in wall-jet flows depicting a boundary layer close to the bottom. Turbulence levels up to 400% were reached, and they decayed with increasing distance from the jump toe. At a given cross-section, the smallest turbulent levels were observed close to the bed whereas the largest values were observed close to the free surface. This was likely caused by the boundary conditions indicating the strong influence of the free surface on the turbulent structure of the flow;
– Lastly, some turbulence time scales were documented showing larger time scales far from the bed and shorter lifetime when the distance from the toe increased.

These results, not available in the literature prior to this study, bring new interesting information in many applications in terms of environmental flows. They should contribute to a better knowledge of the complex phenomena occuring in such flows. For instance, in terms of turbulence and bubble chords, they give new insights into the microscopic structure of the flow as well as on turbulence-bubbles interactions.

The air–water flow is associated with turbulence which can also lead to sediment transport. Note that the turbulence may be strongly affected by bubble dynamics. Physically, the mechanisms involved in these processes are complex (mixing of sediments, air and water). Careful attention must be devoted to scour and sediment transport that can occur with the hydraulic jump formation, which leads to some increase in turbulence level and in bed shear stresses. In these flows, turbulent eddies also develop, grow and propagate. Thus, the threshold of the sediment transport (bed or suspended-load motion) can be locally reached with unexpected consequences (scour, damage, embankment safety etc). Solid par-

ticles and materials can be advected over a large distance with potential consequences for the environment. This justifies the need for further studies of the flow dynamics in hydraulic jumps to improve basic knowledge, to validate numerical models and thus to develop remedial solutions against flood damages and for river restoration and beach management. A better knowledge would help engineers to design new hydraulic structures that maximise energy dissipation [14] and to anticipate any damages that could affect the river and the surrounding landscape characteristics (dam overtopping, flood events etc). It is especially important to identify the most influencing parameters such as the turbulence properties (time and length scales), the Froude number, the Reynolds number, the water depth or the bottom roughness. Note that the boundary conditions (at the bottom and at the air/water interface) are relevant parameters as well. Many numerical and experimental studies actually focus on this turbulence/bubble interaction. For instance, previous studies suggested that some kinetic energy dissipation can be transferred to the entrained air bubbles in the form of some transfer of potential energy [13,15,16]. This experimental work was also relevant to discuss the influence of the free surface on the turbulence properties.

It is well-known that further developments are needed with larger Froude numbers and/or different boundary conditions. An interesting point could also consist in a numerical modelling of the flow, and the present data sets may be a valuable validation test. Some measurements could concern the effect of bottom roughness on the turbulent properties. Comparisons and analysis with previous measurements would also be interesting to assess scale effects between laboratory and field measurements.

References

1. Carosi G, Chanson H (2006) Air–water time and length scales in skimming flows on a stepped spillway. Application to the spray characterization, Report CH59/06. Division of Civil Engineering, The University of Queensland, Brisbane, Australia, July, 142 pp, ISBN 1864998601
2. Chanson H (1995) Air entrainment in two dimensional turbulent shear flows with partially developed inflow conditions. Int J Multiph Flow 21(6):1107–1121. doi:10.1016/0301-9322(95)00048-3
3. Chanson H (1997) Air bubble entrainment in free-surface turbulent shear flows. Academic press, London, 401 pp
4. Chanson H (2002) Air–water flow measurements with intrusive phase detection probes. Can we improve their interpretation? J Hydraul Eng 128(3):252–255. doi:10.1061/(ASCE)0733-9429(2002)128:3(252)
5. Chanson H (2004) The hydraulics of open channel flows: an introduction, 2nd edn. Butterworth-Heinemann, Oxford, 630 pp
6. Chanson (2006) Air bubble entrainment in hydraulic jumps. Similitude and scale effects. Report CH57/05. Department of Civil Engineering, The University of Queensland, Brisbane, Australia, January, 119 pp
7. Chanson H (2007a) Bubbly flow structure in hydraulic jump. Eur J Mech B-Fluids 26(3):367–384. doi:10.1016/j.euromechflu.2006.08.001
8. Chanson H (2007b) Dynamic similarity and scale effects affecting air bubble entrainment in hydraulic jumps. Proceedings of 6th international conference on multiphase flow, ICMF 2007. Leipzig Germany, Session 7
9. Chanson H, Brattberg T (1997) Experimental investigations of air bubble entrainment in developing shear layer. Report CH48/97. Department of civil Engineering, The University of Queensland, Brisbane, Australia, October, 309 pp
10. Chanson H, Brattberg T (2000) Experimental study of the air–water shear flow in a hydraulic jump. Int J Multiph Flow 26(4):583–607. doi:10.1016/S0301-9322(99)00016-6

11. Chanson H, Carosi G (2007) Advanced post-processing and correlation analysis in high-velocity air–water flows. Environ Fluid Mech 7:495–508. doi:10.1007/s10652-007-9038-3
12. Crowe C, Sommerfield M, Tsuji Y (1998) Multiphase flows with droplets and particles. CRC Press, Boca Raton, 471 pp
13. Fuhrboter A (1970) Air entrainment and energy dissipation in breakers. Proceedings of international conference on coastal engineering, pp 391–398
14. Hager WH (1992) Energy dissipators and hydraulic jump. Kluwer Academic Publishers, Water Science and Technology Library, vol 8. Dordrecht, 288 pp
15. Hoque A, Aoki SI (2005) A quantitative analysis of energy dissipation among three typical air entrainment phenomena. Environ Fluid Mech 5:325–340. doi:10.1007/s10652-005-3258-1
16. Hwung HH, Chyan JM, Chung YC (1992) Energy dissipation and air bubbles mixing inside surf zone. Proceedings of 23rd international conference on coastal engineering, vol 1, chap 22. ASCE, Venice, pp 308–321
17. Kucukali S, Chanson H (2007) Turbulence in hydraulic jumps: experimental measurements. Research report CH62/07. Department of Civil Engineering, The University of Queensland, Brisbane, Australia, July, 96 pp, ISBN 9781864998825
18. Liu M, Rajaratnam N, Zhu D (2004) Turbulence structure of hydraulic jumps of low Froude numbers. J Hydraul Eng 130(6):511–520. doi:10.1061/(ASCE)0733-9429(2004)130:6(511)
19. Mossa M, Tolve U (1998) Flow visualization in bubbly two phase hydraulic jumps. J Fluids Eng ASME 120:160–165. doi:10.1115/1.2819641
20. Mouazé D, Murzyn F, Chaplin JR (2004) Turbulence at free surface in hydraulic jumps. Proceedings of 2004 ASME heat transfer/fluids engineering summer conference, Charlotte, USA. Paper No. 56077, 5 pp
21. Mouazé D, Murzyn F, Chaplin JR (2005) Free surface length scale estimation in hydraulic jumps. J Fluids Eng ASME 127:1191–1193. doi:10.1115/1.2060736
22. Murzyn F (2002) Etude de l'influence d'une onde sur les échelles de turbulence: application à la houle. PhD Thesis, University of Cane-Basse Normandie (France), 201 pp (in French)
23. Murzyn F, Chanson H (2007) Free surface, bubbly flow and turbulence measurements in hydraulic jumps, Report CH63/07. Division of Civil Engineering, The University of Queensland, Brisbane, Australia, July, 116 pp. ISBN 9781864998917
24. Murzyn F, Mouazé D, Chaplin JR (2005) Optical fibre probe measurements of bubbly flow in hydraulic jumps. J Multiph Flow 31(1):141–154. doi:10.1016/j.ijmultiphaseflow.2004.09.004
25. Murzyn F, Mouazé D, Chaplin JR (2007) Air–water interface dynamic and free surface features in hydraulic jumps. J Hydraul Res IAHR 45(5):679–685
26. Rajaratnam N (1962) An experimental study of air entrainment characteristics of the hydraulic jump. J Instrum Eng India 42(7):247–273
27. Rajaratnam N (1965) The hydraulic jump as a wall jet. J Hyd Div ASCE 91(HY5):107–132, discussion: 92(HY3):110–123, 93(HY1):74–76
28. Resch FJ, Leutheusser HJ (1972a) Le ressaut hydraulique: mesure de turbulence dans la région diphasique. Houille Blanche 4:279–293 (in French)
29. Resch FJ, Leutheusser HJ (1972b) Reynolds stress measurements in hydraulic jumps. J Hydraul Res IAHR 10(4):409–429
30. Rouse H, Siao TT, Nagaratnam S (1959) Turbulence characteristics of the hydraulic jump. Trans ASCE 124:926–966
31. Toombes L (2002) Experimental study of air–water flow properties on low-gradient stepped cascades. PhD Thesis, Department of Civil Engineering, The University of Queensland, 304 pp